Impact of non-linear resonators in periodic structures using a perturbation approach

M.A. Campana[a,c], M. Ouisse[c], E. Sadoulet-Reboul[c], M. Ruzzene[d], S. Neild[a,b], F. Scarpa[a,b]

[a] *Bristol Composite Institute, University of Bristol, Bristol BS8 1TR, UK*
[b] *Dynamics and Control Research Group (DCRG), Civil. Aerospace and Mechanical Engineering (CAME), University of Bristol, BS8 1TR Bristol, UK*
[c] *Univ. Bourgogne Franche-Comté, FEMTO-ST Department of Applied Mechanics, CNRS/UFC/ENSMM/UTBM, Besançon 25000, FR*
[d] *School of Aerospace Engineering, Georgia Institute of Technology, Atlanta GA 30332, USA*

Abstract

The work describes the wave propagation in a periodic structure formed by a linear spring-mass chain with local Duffing non-linear resonators. The wave propagation is studied using the Floquet-Bloch theorem combined with a perturbation approach to identify the dispersion relations in the nonlinear periodic structure. The theoretical model is benchmarked by a numerical model that considers an analogous finite resonant spring-mass system. The numerical non-linear model provides an apparent dispersion relation of the structure obtained from an inverse identification method, the latter based on imposing a wave number as an initial condition, and then obtaining the corresponding frequency from the analysis of the chain amplitude in the time domain. The perturbation and the numerical methods are compared to discuss the behaviour of the wave propagation in the nonlinear resonators periodic chain.

Keywords: Periodic structures, Resonators, Non-linearities

1. Introduction

The Floquet-Bloch theorem is widely used to investigate the wave propagation in periodic structures, initially introduced in mathematics by Floquet for [1], before being extended in structures [2, 3] and damped systems [4]. Floquet-Bloch provides the dispersion relation of an assumed infinite periodic structure

by analysing the periodic unit cell only. One of the main interests for analysing the wave propagation in these periodic media is to identify "stop bands" or "bandgaps", i.e. frequency areas in which waves are no longer free to propagate. The knowledge of these areas in the wave number/frequency maps can be used to build frequency filters using periodic systems and to create therefore frequency bands in which wave propagation is strongly attenuated. Two types of stop bands can be identified in periodic systems. Bragg bandgaps, related to the material properties or the geometry of the unit cell, and resonant bandgaps, caused by a resonating system included in the periodic structure. In a one dimensional spring-mass resonant system, the combination of a resonating mass with the mass of the principal chain results to an apparent frequency-dependent mass, which has the specificity to become negative for a certain range of frequencies close to the eigenfrequency of the resonator. This phenomena is called negative mass effect [5], and it is related to the presence of a bandgap in those systems.

Several studies have been performed by using resonators systems in periodic structures. Examples are multi-resonators in a single unit cell [6], or the effect of a graded metamaterial [7] to generate pseudo-periodic systems. A large portion of studies related to wave propagation in periodic arrays (also including damping effects) have been described and reviewed in [8]. Some studies have also focused on beam sandwich structures composed by homogenised continuum media with local resonators [9]. Qian [10] has investigated two-dimensional periodic sandwich plate continuum systems using resonators between the two skin panels. Studies about periodic non-linear systems have been performed to observe the effect of the amplitude of the response during wave propagation, and more specifically on the boundaries of the bandgap compared to a linear periodic system. Non-linear resonators in a linear periodic chain have been investigated in previous studies. Lazarov and Jensen [11] have used an harmonic balance method to analyse the asymptotic behaviour of the relative displacement between the principal mass and the resonant mass. Georgiou and Valakis [12] have used a different type of oscillator using an geometric non-linearity originating from the

angle of a pendulum attached to the principal mass of the chain.

The work presented in this paper focuses on developing a formulation to identify the dispersion curve of a non-linear resonator using the perturbation method developed by Nasiretti et al [13] for discrete non-linear spring-mass systems, and then extended to finite element structures by Manktelow et al [14]. The method has been so far applied to a full nonlinear periodic system, and here the behaviour of the nonlinear resonator only is analysed to observe the impact of the eigenfrequency of the resonant system in the corrected term of the dispersion relation. Another novelty presented in this work is the development of a numerical inverse method used on a finite periodic chain structure to obtain the dispersion relation. The method consists in imposing the wave number to the whole chain and then obtain the corresponding frequency analyzing the temporal signal obtained after releasing the system. This method is different from usually applied approaches that consist on imposing an excitation and identifying back the wave number [15], and has the particularity to avoid space aliasing as well as control the amplitude we want to impose to be compared with the perturbation technique. Also, the precise observation of the boundaries of the bandgap can be performed since the wavenumber is imposed.

2. Dispersion analysis for infinite periodic structures

This section details strategies to determine dispersion relations for infinite periodic structures : the case of a linear spring resonator is first considered, then more attention is dedicated to the case of a nonlinear spring-mass resonator.

2.1. Linear spring-mass resonator

Let consider a one-dimensional principal periodic chain made of spring-mass units (mass m and stiffness k). A resonator represented by another spring-mass system (mass m_R and stiffness k_R) is attached to each mass. This chain is considered as infinite, and an appropriate unit cell is defined to apply the Floquet-Bloch Theorem (Fig. 1).

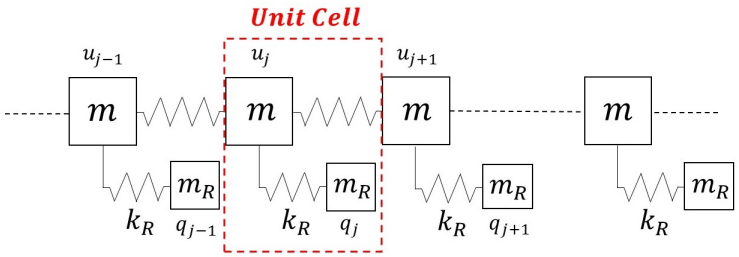

FIGURE 1: 1D resonant spring mass system

By writing the equation of motion of the unit cell linked to its neighbours we obtain the following expression :

$$\begin{cases} m\frac{d^2u_j}{dt^2} + k(2u_j - u_{j-1} - u_{j+1}) - k_R(q_j - u_j) = 0 \\ m_R\frac{d^2q_j}{dt^2} + k_R(q_j - u_j) = 0 \end{cases} \tag{1}$$

where u_j and q_j respectively denote the displacements of the j^{th} principal mass and the j^{th} resonator. In harmonic regime the displacements can be expressed as $x_j = X_j e^{i\omega t}$, with i being a complex number such as $i^2 = -1$. Eq. 1 becomes :

$$\begin{cases} -\omega^2 m u_j + k(2u_j - u_{j-1} - u_{j+1}) - k_R(q_j - u_j) = 0 \\ -\omega^2 m_R q_j + k_R(q_j - u_j) = 0 \end{cases} \tag{2}$$

The term q_j depends on u_j from the second line of Eq. 2. By applying the Floquet-Bloch Theorem to the first line ($u_{j+1} = e^{j\mu}u_j$) (μ being the reduced wave number) one can obtain the following dispersion equation :

$$-m\omega^2 + 2k(1 - \cos(\mu)) + (k_R - \frac{k_R^2}{k_R - m_R\omega^2}) = 0 \tag{3}$$

The roots of Eq. 3 are ω_1 and ω_2, representing the two branches of the

dispersion curve :

$$\begin{aligned}\omega_1 &= \sqrt{\frac{(m+m_R)\Omega_R^2+4k\sin^2(\mu/2)-\sqrt{((m+m_R)\Omega_R^2+4k\sin^2(\mu/2))^2-16km\sin^2(\mu/2)\Omega_R^2}}{2m}}\\ \omega_2 &= \sqrt{\frac{(m+m_R)\Omega_R^2+4k\sin^2(\mu/2)+\sqrt{((m+m_R)\Omega_R^2+4k\sin^2(\mu/2))^2-16km\sin^2(\mu/2)\Omega_R^2}}{2m}}\end{aligned} \tag{4}$$

with $\Omega_R = \sqrt{\frac{k_R}{m_R}}$ being the eigenfrequency of the resonator. The dispersion curve is shown Fig. 2a, with the propagative part in red and the evanescent part in blue for $m_R = m = 1\ kg$ and $k_R = k = 1\ N.m^{-1}$. To validate numerically the result, a finite spring-mass chain of 20 unit cells has been simulated to obtain the Frequency Response Function (FRF) of the system. The boundary conditions in the numerical model are representative of a free-free state at the two extremities of the chain, while the mass located in one of the ends is excited by imposing a longitudinal propagating wave generated by the force $F = F_0\cos(\omega t)$ with $F_0 = 1N$. An harmonic analysis is performed by varying the value of ω, and the amplitude of the displacement is captured on the mass at the other end of the structure. The results are shown in Fig. 2b.

The FRF exhibits the presence of a frequency region in which the amplitude is considerably attenuated. This area represents the bandgap (resonant in this case). A resonant bandgap can be differentiated from a Bragg one by observing the boundaries of the propagating part [16]. In the resonant case, a wave will stop propagating for a value of $\mu = \pi$ and then propagates again for $\mu = 0$. The boundaries of the bandgap can be expressed by calculating the values of $\omega_1(\mu = \pi)$ and $\omega_2(\mu = 0)$, leading to the following expression :

$$\begin{aligned}\omega_g^2 &= \frac{(m+m_R)\Omega_R^2+4k-\sqrt{((m+m_R)\Omega_R^2+4k)^2-16km\Omega_R^2}}{2m}\\ \omega_d^2 &= \Omega_R^2(1+\tfrac{m_R}{m})\end{aligned} \tag{5}$$

with ω_g and ω_d being the pulsation of the left and the right boundary, respectively. It is also important to notice that the value of Ω_R is bounded by the values of ω_g and ω_d, and this has consequences on the value of the amplitude of the resonant mass. The rewriting of the second line of Eq. 2 leads to $q_j = \frac{\Omega_R^2}{\Omega_R^2-\omega^2}u_j$. This expression indicates that the value of the amplitude of q_j

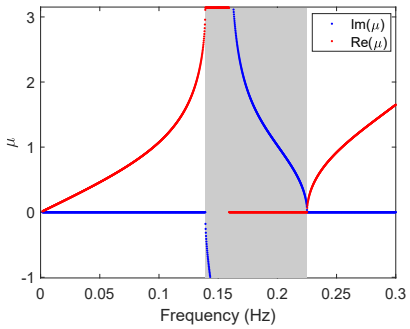

(a) Dispersion curve for the infinite structure. Propagative part in red ($Re(\mu)$) and evanescent part in blue ($Im(\mu)$)

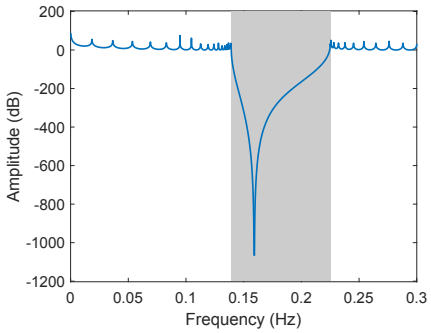

(b) Forced Response Frequency at one of the extremity of a finite structure of 20 unit cells

FIGURE 2: Results for one dimensional linear resonant spring-mass system

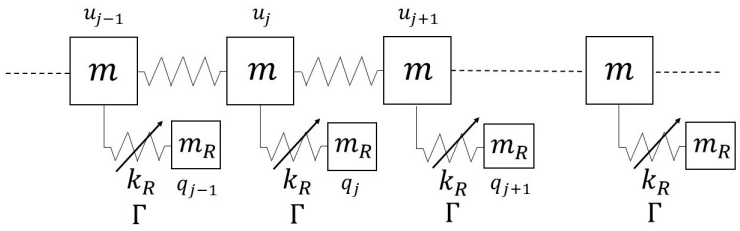

FIGURE 3: 1D non-linear resonant spring mass system

strongly depends on the value of Ω_R for an fixed value of the u_j amplitude. The term q_j will however never be able to reach an infinite value in the propagative zone, since $\omega^- < \omega_g < \Omega_R < \omega_d < \omega^+$, with ω^- and ω^+ representing respectively the value of the pulsation before ω_g and after ω_d. This property of a resonating system is different from a representation of spring-mass systems with Bragg bandgaps, like the diatomic mass system of Hussein et al. [17]. This particular periodic configuration shows amplitudes of the two masses that depend directly to the boundaries of the bandgap. This may have repercussions for the representation on the nonlinear system.

2.2. Nonlinear spring-mass resonator system

2.2.1. Perturbation method for identification of non-linear dispersion diagram

A Duffing spring mass resonator is added between the masses m and m_R. In this case the non-linear force is expressed as :

$$f_{nl} = k_R(q_j - u_j) + \varepsilon\Gamma(q_j - u_j)^3 \tag{6}$$

where Γ is the nonlinear stiffness constant and ε a small perturbation parameter. Replacing f_{nl} in Eq. 1 leads to :

$$\begin{cases} m\frac{d^2u_j}{dt^2} + k(2u_j - u_{j-1} - u_{j+1}) - k_R(q_j - u_j) - \varepsilon\Gamma(q_j - u_j)^3 = 0 \\ m_R\frac{d^2q_j}{dt^2} + k_R(q_j - u_j) + \varepsilon\Gamma(q_j - u_j)^3 = 0 \end{cases} \tag{7}$$

The objective here is to idenify the correction term in the dispersion relation using the Lindstedt-Poincaré adapted method developed in [13]. The main goal

is to generate a first order asymptotic development on the displacements of the masses and on the frequency, corresponding to the following expressions :

$$\begin{aligned} u_j &= u_j^{(0)} + \varepsilon u_j^{(1)} + O(\varepsilon^2), \\ q_j &= q_j^{(0)} + \varepsilon q_j^{(1)} + O(\varepsilon^2), \\ \omega &= \omega_0 + \varepsilon \omega_1 + O(\varepsilon^2). \end{aligned} \tag{8}$$

Replacing expressions 8 in Eq. 7 gives, after development and separation of the equations in the ε^0 and ε^1 orders :

$$\varepsilon^0 : \begin{cases} \underline{\omega}_0^2 \frac{d^2 u_j^{(0)}}{d\tau^2} + (2u_j^{(0)} - u_{j-1}^{(0)} - u_{j+1}^{(0)}) - \beta(q_j^{(0)} - u_j^{(0)}) = 0, \\ \kappa^2 \underline{\omega}_0^2 \frac{d^2 q_j^{(0)}}{d\tau^2} + (q_j^{(0)} - u_j^{(0)}) = 0, \end{cases} \tag{9}$$

$$\varepsilon^1 : \begin{cases} \underline{\omega}_0^2 \frac{d^2 u_j^{(1)}}{d\tau^2} + (2u_j^{(1)} - u_{j-1}^{(1)} - u_{j+1}^{(1)}) - \beta(q_j^{(1)} - u_j^{(1)}) = -2\underline{\omega}_0 \underline{\omega}_1 \frac{d^2 u_j^{(0)}}{d\tau^2} + \bar{\Gamma}(q_j^{(0)} - u_j^{(0)})^3 \\ \kappa^2 \underline{\omega}_0^2 \frac{d^2 q_j^{(1)}}{d\tau^2} + (q_j^{(1)} - u_j^{(1)}) = -2\kappa^2 \underline{\omega}_0 \underline{\omega}_1 \frac{d^2 q_j^{(0)}}{d\tau^2} - \frac{\bar{\Gamma}}{\beta}(q_j^{(0)} - u_j^{(0)})^3 \end{cases} \tag{10}$$

with $\underline{\omega}_n^2 = \frac{\omega_n^2}{\Omega_0^2}$, $\Omega_0^2 = \frac{k}{m}$, $\alpha = \frac{m_R}{m}$, $\beta = \frac{k_R}{k}$, $\kappa = \sqrt{\frac{\alpha}{\beta}}$, $\bar{\Gamma} = \frac{\Gamma}{k}$, $\tau = \omega t$. Assuming an harmonic regime is reached, the displacements $u_j^{(0)}$ and $q_j^{(0)}$ can be expressed in the following form :

$$\begin{aligned} u_j^{(0)} &= \tfrac{A_u}{2} e^{ji\mu} e^{i\tau} + \tfrac{\bar{A_u}}{2} e^{-ji\mu} e^{-i\tau} \\ q_j^{(0)} &= \tfrac{A_q}{2} e^{ji\mu} e^{i\tau} + \tfrac{\bar{A_q}}{2} e^{-ji\mu} e^{-i\tau} \end{aligned} \tag{11}$$

The second order derivatives are then :

$$\begin{aligned} \tfrac{d^2 u_j^{(0)}}{d\tau^2} &= -u_j^{(0)} \\ \tfrac{d^2 q_j^{(0)}}{d\tau^2} &= -q_j^{(0)} \end{aligned} \tag{12}$$

Replacing Eq. 11 and 12 into Eq. 9 yields

$$\varepsilon^0 : \begin{cases} -\underline{\omega_0^2} u_j^{(0)} + (2u_j^{(0)} - u_{j-1}^{(0)} - u_{j+1}^{(0)}) - \beta(q_j^{(0)} - u_j^{(0)}) = 0 \\ -\kappa^2 \underline{\omega_0^2} q_j^{(0)} + (q_j^{(0)} - u_j^{(0)}) = 0 \end{cases} \tag{13}$$

Eq. 13 is equivalent to Eq. 2. Following the same process as in the linear case, roots are now expressed as

$$\begin{aligned}(\underline{\omega}_0^{(1)})^2 &= \frac{1+\alpha+4\kappa^2\sin^2(\frac{\mu}{2})-\sqrt{(1+\alpha+4\kappa^2\sin^2(\frac{\mu}{2}))^2-16\kappa^2 sin^2(\frac{\mu}{2})}}{2\kappa^2},\\ (\underline{\omega}_0^{(2)})^2 &= \frac{1+\alpha+4\kappa^2\sin^2(\frac{\mu}{2})+\sqrt{(1+\alpha+4\kappa^2\sin^2(\frac{\mu}{2}))^2-16\kappa^2 sin^2(\frac{\mu}{2})}}{2\kappa^2}.\end{aligned} \tag{14}$$

When adopting the same approach used during the linear analysis, the purpose is to isolate the corrected displacement $q_j^{(1)}$ in the second line of Eq. 10 and inject it in the first line. In this way it is possible to obtain all the nonlinear terms in the same equation. To do so, it is assumed that the displacement $q_j^{(1)}$ can be expressed under the form :

$$q_j^{(1)} = Be^{i\tau} + \bar{B}e^{-i\tau} \tag{15}$$

Where B the amplitude of $q_j^{(1)}$, whose the value does not have importance for the following calculations. Replacing Eq. 15 in the second line of Eq. 10 we obtain :

$$\varepsilon^1 : \begin{cases} \underline{\omega}_0^2 \frac{d^2u_j^{(1)}}{d\tau^2} + (2u_j^{(1)} - u_{j-1}^{(1)} - u_{j+1}^{(1)}) - \beta(q_j^{(1)} - u_j^{(1)}) = -2\underline{\omega}_0\underline{\omega}_1 \frac{d^2u_j^{(0)}}{d\tau^2} + \bar{\Gamma}(q_j^{(0)} - u_j^{(0)})^3 \\ q_j^{(1)} = \frac{1}{1-\kappa^2\underline{\omega}_0^2}(u_j^{(1)} - 2\kappa^2\underline{\omega}_0\underline{\omega}_1 \frac{d^2q_j^{(0)}}{d\tau^2} - \frac{\bar{\Gamma}}{\beta}(q_j^{(0)} - u_j^{(0)})^3) \end{cases} \tag{16}$$

By injecting expression of $q_j^{(1)}$ in the first line of Eq. 10 we have :

$$\underline{\omega}_0^2 \frac{d^2u_j^{(1)}}{d\tau^2} + (2u_j^{(1)} - u_{j-1}^{(1)} - u_{j+1}^{(1)}) - \beta\frac{\kappa^2\underline{\omega}_0^2}{1-\kappa^2\underline{\omega}_0^2}u_j^{(1)} = F(\tau) \tag{17}$$

with :

$$F(\tau) = 2\underline{\omega}_0\underline{\omega}_1 \frac{\alpha + (1-\kappa^2\underline{\omega}_0^2)^2}{(1-\kappa^2\underline{\omega}_0^2)^2} u_j^{(0)} - \bar{\Gamma}\left(\frac{\kappa^2\underline{\omega}_0^2}{1-\kappa^2\underline{\omega}_0^2}\right)^4 (u_j^{(0)})^3 \tag{18}$$

Replacing $u_j^{(0)}$ by its expression 11, the equation becomes :

$$F(\tau) = \left(\underline{\omega}_0\underline{\omega}_1 \frac{\alpha + (1-\kappa^2\underline{\omega}_0^2)^2}{(1-\kappa^2\underline{\omega}_0^2)^2} A_u - \frac{3\bar{\Gamma}}{8}\left(\frac{\kappa^2\underline{\omega}_0^2}{1-\kappa^2\underline{\omega}_0^2}\right)^4 A_u^2\bar{A}_u\right)e^{i\tau}e^{ij\mu} + d_1e^{3i\tau}e^{3ij\mu} \tag{19}$$

The terms d_1 are associated to the 3^{rd} order of the nonlinearity. The linear kernel of Eq. 17 is similar to the one in Eq. 3 ; this implies that one needs to have all the coefficients in $e^{ij\mu}$ must be equal to 0 not to obtain a secular term in the temporal expression of $u_j^{(1)}$. By imposing this condition and rearranging the equation, we obtain the following expression for $\underline{\omega}_1$:

$$\underline{\omega}_1 = \frac{3\bar{\Gamma}|A_u|^2}{8} \frac{\kappa^8 \underline{\omega}_0^7}{(1-\kappa^2\underline{\omega}_0^2)^2(\alpha+(1-\kappa^2\underline{\omega}_0^2)^2)} \tag{20}$$

Equation 20 leads to the establishment of the final expression describing the corrected dispersion relation for the periodic structure :

$$\underline{\omega}^{(p)} = \underline{\omega}_0^{(p)} + \varepsilon \frac{3\bar{\Gamma}|A_u|^2}{8} \frac{\kappa^8 (\underline{\omega}_0^{(p)})^7}{(1-\kappa^2(\underline{\omega}_0^{(p)})^2)^2(\alpha+(1-\kappa^2(\underline{\omega}_0^{(p)})^2)^2)} \tag{21}$$

with $p = 1$ representing the left branch, and $p = 2$ being the right branch of the dispersion curve. Eq. 21 illustrates the importance of the pulsation of the resonator to determine the value of ω_1. If $\kappa^2\underline{\omega}_0^2$ approaches 1 (i.e., equivalent to say that ω approaches Ω_R), the value of $\underline{\omega}_1$ will increase and might reach a point where it becomes greater than $\underline{\omega}_0$. This would however contradict the hypothesis underlying the current perturbation method. That condition shows that the value of the parameters for the resonators plays a crucial role in the distance that Ω_R must possess compared to the boundaries of the bandgap.

During the following analyses we will consider the parameters α,κ, $\bar{\Gamma}$ are considered to be equal to 1 (unless $\bar{\Gamma} = 0$, and this to obtain the linear case). The graphic representation of the corrected dispersion curve obtained is shown Fig. 4.

2.2.2. Domain of amplitude validity

The perturbation analysis assumes an asymptotic development of the term $\underline{\omega}$ to obtain the nonlinear corrected result. However, the asymptotic development of the term $\underline{\omega}^2 = (\underline{\omega}_0 + \varepsilon\underline{\omega}_1)^2 = \underline{\omega}_0^2 + 2\varepsilon\underline{\omega}_0\underline{\omega}_1$ leading to Eq. 10 is true only if $2\varepsilon\underline{\omega}_0\underline{\omega}_1 \ll \underline{\omega}_0^2$, which can be rewritten as $2\varepsilon\frac{\underline{\omega}_1}{\underline{\omega}_0} \ll 1$. $\underline{\omega}_1$ is replaced in Eq. 21

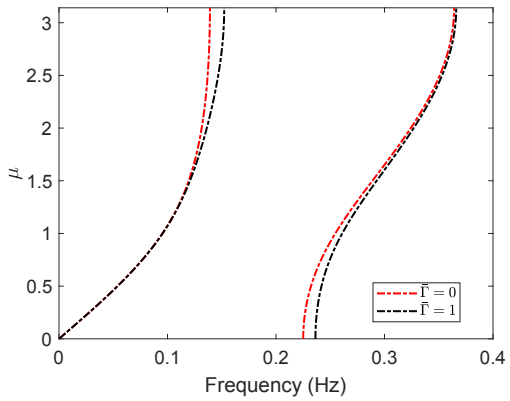

FIGURE 4: Dispersion curve using the perturbation approach in the nonlinear case for $A_u = 1$ and $\varepsilon = 0.05$

leading to the following condition :

$$\frac{3|A_u|^2\varepsilon}{4}\frac{\underline{\omega}_0^6}{(1-\underline{\omega}_0^2)^2(1+(1-\underline{\omega}_0^2)^2)} \ll 1 \tag{22}$$

By assuming that the order of magnitude of $\ll$ is the same as ε, the following condition for the amplitude can be written :

$$|A_u|h(\underline{\omega}_0) < 1 \tag{23}$$

where $h(\underline{\omega}_0) = \sqrt{\frac{3}{4}\frac{\underline{\omega}_0^6}{(1-\underline{\omega}_0^2)^2(1+(1-\underline{\omega}_0^2)^2)}}$. Plotting the function $\frac{1}{h}$ will give the maximum admissible value that $|A_u|$ can assume to satisfy the equation 23. The results are shown figure 5. Fig. 5a shows that for values of μ up to 1.0 almost any value of A_u would not affect the dispersion in the nonlinear regime. This means that the hypothesis of linearisation will be true, even for very high values of amplitude. However, the amplitude results to be much lower when the wave number increases, approaching a maximum theoretical limit of 0.48. The opposite behaviour however happens in the right branch (Fig. 5b) ; in this case it is possible to observe a limit for A_u, with a minimum value around 0.6 in the low wave numbers ranger and reaching 1.8 for high values of μ.

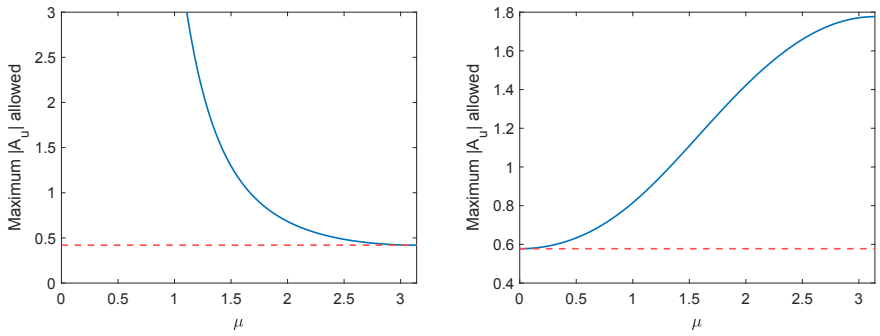

(a) Value of $\frac{1}{h(\underline{\omega}_0)}$ for the left branch of the dispersion curve $(\underline{\omega}_0^{(1)})$

(b) Value of $\frac{1}{h(\underline{\omega}_0)}$ for the right branch of the dispersion curve $(\underline{\omega}_0^{(2)})$

FIGURE 5: Maximum of amplitude versus wave number analysis

3. Identification of dispersion curves from analysis of finite nonlinear periodic structures

This section presents a numerical method to obtain the apparent wave number of the structure, followed then by results related to this approach and a comparison with the method described in 2.

3.1. Inverse method

In general the techniques used to identify the apparent wave number of a periodic structure are based on applying an harmonic excitation to one of the masses of the periodic structure and then evaluating the response.

This paper introduces here other numerical method to compare the results obtained from the perturbation theory. The idea underpinning this methodology is to impose the wave number of the whole structure as an initial condition, releasing the system and observing how it evolves in the time, and then obtain the frequency of the corresponding imposed wavenumber as output. One of the advantages of this novel methodology is that a time-domain analysis is required, rather than the space-domain analysis one to obtain the wave number in direct methods [18]. The use of a time-domain analysis helps to reduce the error made due to the spatial discretisation of the periodic structure. In particular

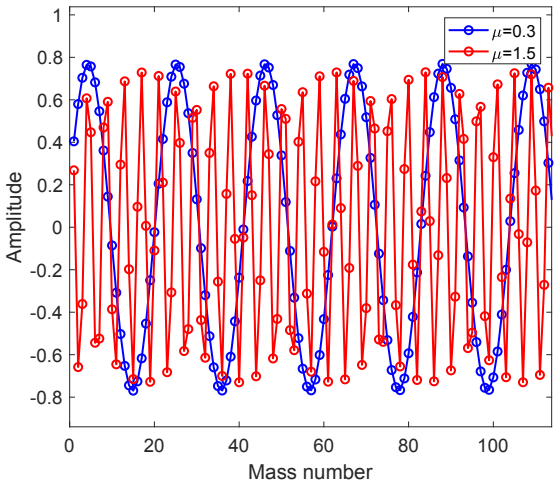

FIGURE 6: Spatial representation of masses for two different values of μ.

for spring-mass systems, the distance between two consecutive masses does not need to be represented in the model, and this allows to fix the element length to unity. According to the Shannon theorem, a minimum of 2 elements per wavelength is necessary to avoid space aliasing. However, to represent a sinusoidal excitation in a correct way, it is common to use at least 6 elements per wavelength, and that condition can not be reached when the wavenumber exceeds 1. Fig. 6 illustrates this problem by showing the space representation for two different wave numbers. It is however important to note that this method fits mainly numerical simulations, since imposing a displacement as an initial conditions could be much less practical in an experiment than imposing an harmonic excitation to the whole structure.

The finite structure here is represented by an assembly of 300 unit cells in a linear chain. The equation of motion of the finite structure with a free-free boundary condition is written and solved using ODE45 in Matlab. A perfectly matched layer (PML) is also used at the boundaries of the structure to avoid wave reflection. The PML consists in a viscous damping force $c(x_p).\dot{x}_p$ applied

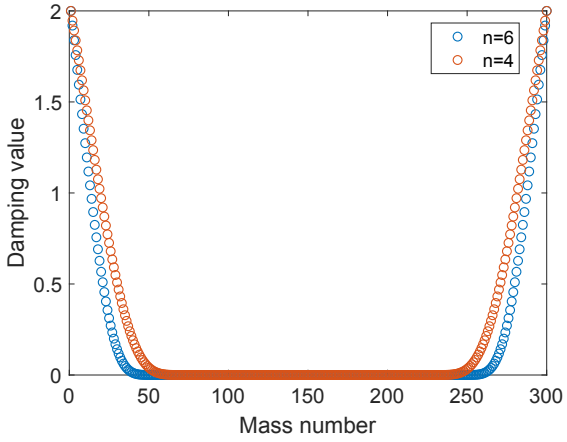

FIGURE 7: Representation of the PML

to all the masses of the principal chain under the form :

$$c(x_p) = Ce^{1-\frac{1}{(1-x_p)^n}} \tag{24}$$

with C a constant positive value, $x_p \in [0;2]$ a value interpolating the mass at the p^{th} position such as $c(0) = c(2) = C$ and $c(1) = 0$, and n an even number representing the order of the PML. The higher the value of n is, the less the masses close to the boundaries will be affected by the damping. Fig. 7 shows the trend of the PML for two different values of n and $C = 2$.

The resolution of the linear system (i.e. with $\Gamma = 0$) is has to be done in order to obtain the values of $\underline{\omega}_0(\mu)$ corresponding to the dispersion curve in the linear case. This step is necessary to impose the initial condition of the resonating system, written as

$$A_q = \frac{A_u}{1 - \kappa^2 \underline{\omega}_0^2}. \tag{25}$$

Those initial conditions are then written under the following form :

$$\begin{cases} U_j(t=0) = A_u \cos(\mu(x_j - x_0)) \\ \dot{U}_j(t=0) = 0 \\ Q_j(t=0) = A_q \cos(\mu(x_j - x_0)) \\ \dot{Q}_j(t=0) = 0 \\ j \in [\![1; 300]\!] \end{cases} \tag{26}$$

The terms U_j and Q_j are the values of the displacements of the j^{th} principal and resonating mass of the system, respectively. The location of the mass considered to obtain the time-displacement response is x_0, and μ is the reduced wave number. The value of x_0 has to be chosen carefully in order to obtain a coherent representation of the results : if the chosen mass is too close to the boundaries, the PML and eventually residual wave reflections will provide incoherent results. For that reason the observed mass should be located in the middle of the structure. Also, even if the displacement is imposed, the spatial discretisation will still be inaccurate for wave numbers greater than one ; this implies however the risk of not always obtaining the maximum value of the amplitude if a random mass is selected as an output. The writing of the initial spatial displacement as in Eq. 26 ensures that the amplitude A_u will be observable for the mass located in x_0 for any value of μ, when $x_j = x_0$.

After the masses being released for an imposed wave number μ_0 and after a time equivalent to $t = 25T_0$ such as $T_0 = \frac{2\pi}{\omega_0(\mu_0)}$, the frequency of the time signal coming from the mass located in x_0 is measured. One example of input and output signal obtained for a $\mu = 1$ on the right branch of the dispersion curve is shown Fig. 8. Fig. 8b shows that the amplitude does not remain constant and equal to A_u as long as the time goes by. Consequently, a Fast Fourier Transform would not give accurate results here, since the obtained signal have variations of amplitude and therefore variations of frequency due to the non-linear behaviour. Alternatively, an average of the periods of the signal is done to get the global value of the frequency. Depending on the imposed wave number, the value of the output average amplitude will become different, which makes not

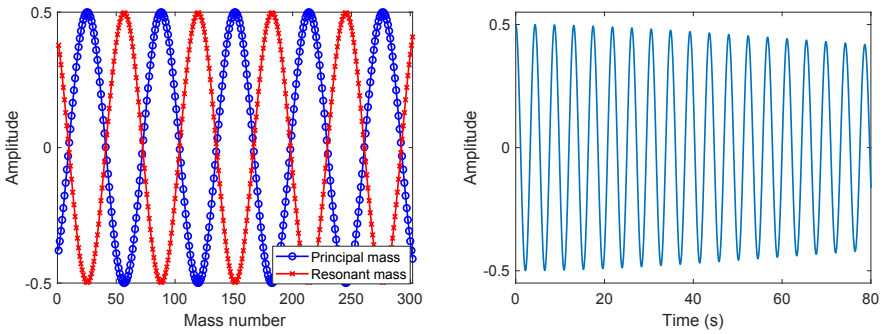

(a) Initial conditions of the system (b) Time signal obtained for the mass x_0

FIGURE 8: Exemple of input and output signal for $A_u = 0.5$ and $\mu = 0.1$

possible a complete comparison with the perturbation method, which assumes a fixed amplitude for every wave number. To fix this problem, an algorithm is implemented, which consists in iterating the simulations starting with an imposed amplitude A_{u0}. The goal of the algorithm is to reach the targeted value A_u by comparing it with the output amplitude of the system (noted A_{out}). After an iteration, the value of A_{out} is estimated performing a Hilbert transform of the signal :

$$A_{out} = |\mathcal{H}(U_0(t))| \tag{27}$$

If $A_{out} < A_u$, the value of A_{u0} is slightly increased and the process is repeated until $A_{out} = A_u$ with a certain tolerance. Once this condition is done, one can capture the average frequency of the signal to obtain the combination (μ, ω). Fig. 8 shows the results using initial conditions shown in Fig. 9, with a value of $A_{u0} = 0.53$ to get an average value $A_{out} = 0.5$. The dashed line represents the value of amplitude equal 0.5.

3.2. Numerical results

Before obtaining the numerical nonlinear dispersion curves, a verification of the condition estimated in subsection 2.2.2 has to be performed to verify that the domain of validity of the amplitudes matches with the prediction when using

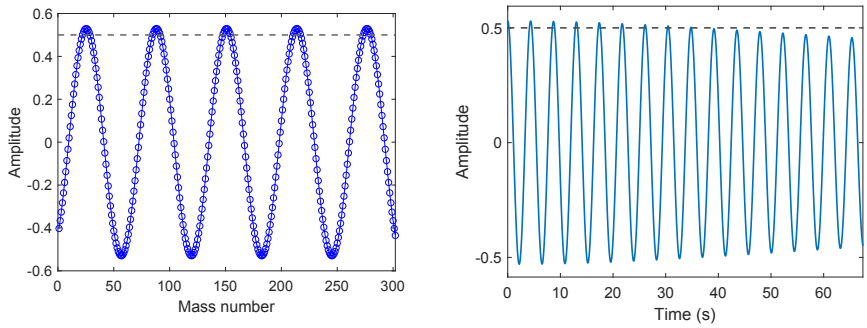

(a) Initial conditions applied to the mass of the principal chain after algorithm

(b) Time signal obtained for the mass x_0 after algorithm

FIGURE 9: Input and output signals obtained after correction

the numerical model. This verification is done by launching numerical simulations with a variation of the amplitude and the wave number in the following domains : $A_u \in [0.1; 0.6]$, $\mu \in [1; \pi]$ for the left branch and $\mu \in [0; \pi]$ for the right branch. The frequency resulting from the simulations are then compared with the frequency computed with the perturbation, and a relative frequency error is calculated as

$$f_{err} = \frac{|f_{num} - f_{per}|}{f_{per}} \tag{28}$$

with f_{num} the frequency obtained with the numerical simulations and f_{per} the frequency obtained with the perturbation method. On the other hand, the value of $2\frac{\omega_0}{\omega_1}$ representing the condition leading to Eq. is calculated 23 is calculated. The highest the value of this function, the higher the error of the perturbation hypothesis. Fig. 10a shows that for high values of μ and amplitudes, the error increases rapidly. This curve actually generalises figure 5a, in which the relative error was fixed to 1, to give an overview of how fast this error is evolving for higher values of amplitude. Fig. 10b shows that the error tends to follow patterns similar to the previous result, and it also shows the same behaviour for high values of amplitude. Similar comments can be provided for the results presented in Fig. 11. Also this case, the error rapidly increases after $A_u \gtrsim 0.3$.

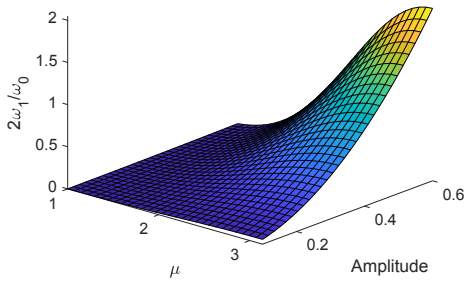

(a) Value of $2\frac{\omega_0}{\omega_1}$ (perturbation method error)

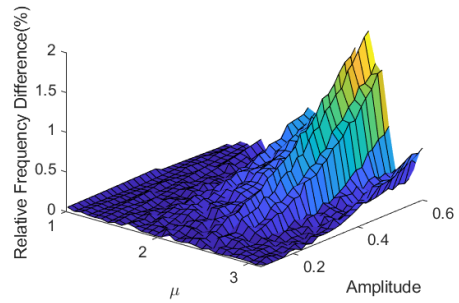

(b) Relative frequency difference between numerical and perturbation method

FIGURE 10: Model error estimation for the left branch of the dispersion curve

Those estimations are close to the ones found with the asymptotic assumption shown in 2.2.2 ; they are however not exactly the same because of the numerical precision of the solver used for the finite structure, and the estimation of taking ε as "small".

The corrected dispersion curve for a amplitude value of $A_u = 0.3$ is represented Fig. 12, and zooms on the branches are shown Fig. 13 and 14. From the close looks it is possible to observe the difference between the numerical method and the perturbation approach. One can observe that for this particular value of amplitude, numerical and theoretical results provide a close match, and the dispersion curve is shifted to higher frequencies compared to the linear case.

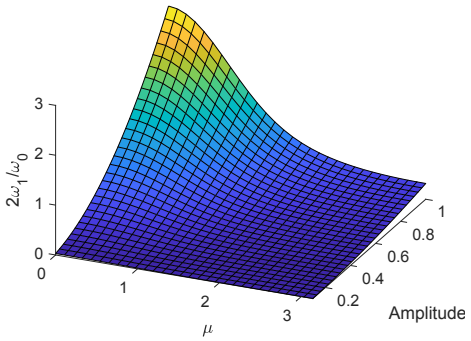

(a) Value of $2\frac{\omega_0}{\omega_1}$ (perturbation method error)

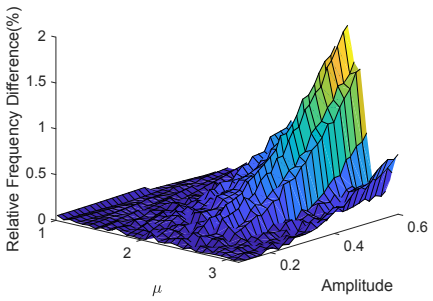

(b) Relative frequency difference between numerical and perturbation method

FIGURE 11: Model error estimation for the right branch of the dispersion curve

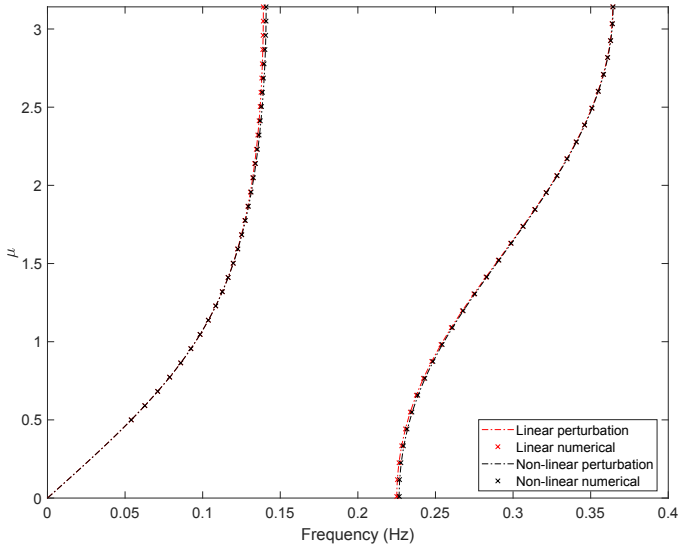

FIGURE 12: Nonlinear dispersion curve ($A_u = 0.3$, $\varepsilon = 0.05$)

This result is consistent with the fact that a nonlinear cubic spring has been added to the model, hence stiffening the structure and increasing value of eigen-
290 frequencies. A result imposing an amplitude for an high amplitude ($A_u = 1.5$) and the time signal associated to the value of $\mu = 0.3$ shown Fig. 15. Fig. 15a demonstrates that the results will be inaccurate up to a certain value of wave-number (around 0.8 in that case) but will still remain correct after this value. Fig.15b confirm that the high level of amplitude does not satisfy the hypothesis
295 of the Lindstet-Poincaré approach.

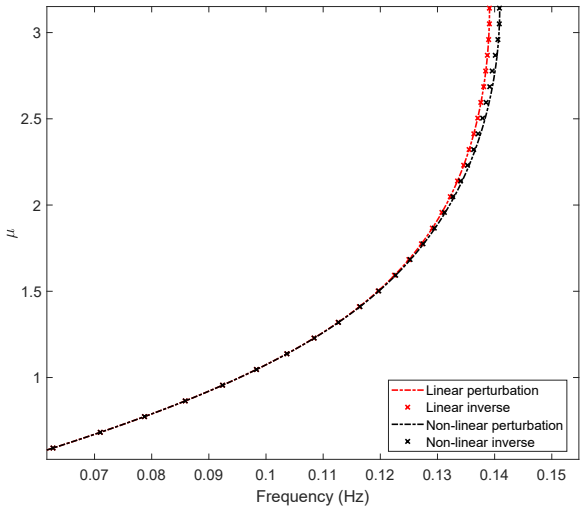

FIGURE 13: Zoom on the left branch of the dispersion curve ($A_u = 0.3$, $\varepsilon = 0.05$)

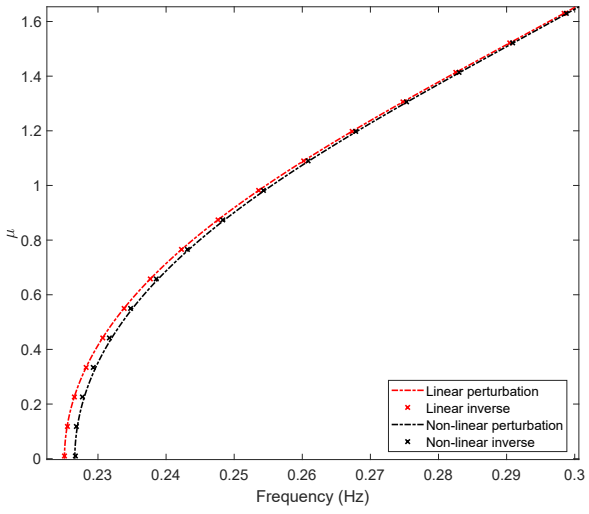

FIGURE 14: Zoom on the right branch of the dispersion curve ($A_u = 0.3$, $\varepsilon = 0.05$)

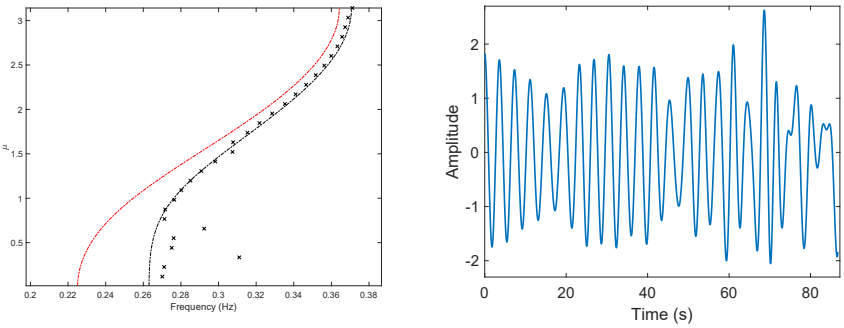

(a) Right branch of the dispersion curve for $A_u = 1.5$

(b) Time signal for $\mu = 0.3$ and a targeted amplitude $A_u = 1.5$

FIGURE 15: Results for an amplitude overpassing the nonlinear assumptions limit

4. Conclusion

Nonlinear periodic resonating systems made of baseline linear chains and distributed Duffing oscillators have been evaluated in this work using a perturbation approach. A quantitative study of the maximum admissible amplitude has been performed to provide an overview of the limits of the proposed method. A new inverse approach imposing the wavenumber has also been developed and applied to a finite structure with a large number of unit cells to confirm the results obtained with the perturbation method. This numerical inverse identification approach provides a different way of analysing the wave propagation of nonlinear periodic structures. The approaches proposed in this work could be also extended to multi dimensional structures, as well as finite element structures to observe the influence of the only resonant part of a system and perform the inverse method in more complex cases.

5. Acknowledgements

This work has been supported by the MSCA ITN VIPER (Vibroacoustics of Periodic Media) programme.

This project has received funding from the European Union's Horizon 2020 research and innovation programme under Marie Curie grant agreement No 675441.

This work was performed in cooperation with the EUR EIPHI program (ANR 17-EURE-0002).

References

[1] G. Floquet, Sur les équations différentielles linéaires à coefficients périodiques, Annales scientifiques de l'École Normale Supérieure 2e série, 12 (1883) 47–88. doi:10.24033/asens.220.
URL http://www.numdam.org/item/ASENS_1883_2_12__47_0

[2] L. Rayleigh, Xvii. on the maintenance of vibrations by forces of double frequency, and on the propagation of waves through a medium endowed with a periodic structure, The London, Edinburgh, and Dublin Philosophical Magazine and Journal of Science 24 (147) (1887) 145–159. doi:10.1080/14786448708628074.

[3] L. Brillouin, Wave Propagation in Periodic Structures., Dover Publication, Inc. NY, 1953.

[4] M. Collet, M. Ouisse, M. Ruzzene, M. Ichchou, Floquet–bloch decomposition for the computation of dispersion of two-dimensional periodic, damped mechanical systems, International Journal of Solids and Structures 48 (20) (2011) 2837 – 2848. doi:https://doi.org/10.1016/j.ijsolstr.2011.06.002.
URL http://www.sciencedirect.com/science/article/pii/S0020768311002125

[5] S. Yao, X. Zhou, G. Hu, Experimental study on negative effective mass in a 1d mass–spring system, New Journal of Physics 10 (4) (2008) 043020. doi:10.1088/1367-2630/10/4/043020.

[6] X. Zhou, W. Jun, R. Wang, J. Lin, Effects of relevant parameters on the bandgaps of acoustic metamaterials with multi-resonators, Applied Physics A (2016) 043020doi:10.1007/s00339-016-9978-x.

[7] A. Banerjee, R. Das, E. P. Calius, Frequency graded 1d metamaterials : A study on the attenuation bands, Journal of Applied Physics 122 (7) (2017) 075101. doi:10.1063/1.4998446.

[8] A. Banerjee, R. Das, E. P. Calius, Waves in structured mediums or metamaterials : A review, Archives of Computational Methods in Engineeringdoi:10.1063/1.4998446.

[9] J. Chen, B. Sharma, C. Sun, Dynamic behaviour of sandwich structure containing spring-mass resonators, Composite Structures 93 (8) (2011) 2120 – 2125. doi:https://doi.org/10.1016/j.compstruct.2011.02.007.

[10] D. Qian, Z. Shi, Bandgap properties in locally resonant phononic crystal double panel structures with periodically attached spring–mass resonators, Physics Letters A 380 (41) (2016) 3319 – 3325. doi:https://doi.org/10.1016/j.physleta.2016.07.068.

[11] B. Lazarov, J. Jensen, Low-frequency band gaps in chains with attached non-linear oscillators, International Journal of Non-Linear Mechanics 42 (10) (2007) 1186.

[12] I. T. Georgiou, A. F. Vakakis, An invariant manifold approach for studying waves in a one-dimensional array of non-linear oscillators, International Journal of Non-Linear Mechanics 31 (6) (1996) 871 – 886, a Selective Perspective on Non-linear Mechanics : Problems and Techniques. doi:https://doi.org/10.1016/S0020-7462(96)00104-7.

[13] R. K. Narisetti, M. Leamy, M. Ruzzene, A perturbation approach for predicting wave propagation in one-dimensional nonlinear periodic structures, Journal of Vibration and Acoustics 132 (2010) 031001–1. doi:10.1115/1.4000775.

[14] K. Manktelow, R. K. Narisetti, M. Leamy, M. Ruzzene, Finite-element based perturbation analysis of wave propagation in nonlinear periodic structures, Mechanical Systems and Signal Processing 39 (2013) 32–46. doi:10.1016/j.ymssp.2012.04.015.

[15] K. L. Manktelow, M. Leamy, M. Ruzzene, Analysis and experimental estimation of nonlinear dispersion in a periodic string, Journal of Vibration and Acoustics 136 (2014) 031016. doi:10.1115/1.4027137.

[16] B. Sharma, C. Sun, Local resonance and bragg bandgaps in sandwich beams containing periodically inserted resonators, Journal of Sound and Vibration 364 (2016) 133 – 146. doi:https://doi.org/10.1016/j.jsv.2015.11.019.

[17] M. Hussein, M. Leamy, M. Ruzzene, Dynamics of phononic materials and structures : Historical origins, recent progress, and future outlook, Applied Mechanics Reviews 66 (2014) 040802. doi:10.1115/1.4026911.

[18] J. Berthaut, M. Ichchou, L. Jezequel, K-space identification of apparent structural behaviour, Journal of Sound and Vibration - J SOUND VIB 280 (2005) 1125–1131. doi:10.1016/j.jsv.2004.02.044.